Effect of Re_λ and Rouse numbers on the settling of inertial droplets in homogeneous isotropic turbulence

Daniel Odens Mora[*] and Martin Obligado[†]
Université Grenoble Alpes, CNRS, Grenoble-INP, LEGI, F-38000 Grenoble, France

Alberto Aliseda
Department of Mechanical Engineering, University of Washington, Seattle, Washington 98195-2600, USA

Alain Cartellier
Université Grenoble Alpes, CNRS, Grenoble-INP, LEGI, F-38000, Grenoble, France

(Received 3 November 2020; accepted 6 April 2021; published 20 April 2021)

We present an experimental study on the settling velocity of dense sub-Kolmogorov particles in active-grid-generated turbulence in a wind tunnel. Using phase Doppler interferometry, we observe that the modifications of the settling velocity of inertial particles, under homogeneous isotropic turbulence and dilute conditions [i.e., small liquid fraction $\phi_v \leqslant O(10)^{-5}$], is controlled by the Taylor-Reynolds number Re_λ of the carrier flow. Meanwhile, we did not find a strong influence of the ratio between the fluid and gravity accelerations on the particle settling behavior. Remarkably, we find that that the degree of hindering experienced by the particles (i.e., the measured particle settling velocity is smaller in magnitude than its respective one in still fluid conditions) increases with Re_λ. This observation is contrary to previous works at intermediate values of Re_λ that report the opposite effect: settling enhancement. Nonetheless, our trend is observed at all particle sizes investigated, and when previous experimental data is included into the analysis, our data suggest that the particle settling behavior may be nonmonotonic with Re_λ: inducing enhancement at moderate values of Re_λ, and at promoting hindering at higher values of Re_λ. Moreover, at the highest Re_λ studied, the settling enhancement regime ceases to exist. Finally, we find that the difference between the measured particle settling velocity (V_p) and the particle terminal velocity in still fluid conditions (V_T), normalized by the carrier phase rms fluctuations, $(V_p - V_T)/u$ scales linearly with the Rouse number $\mathrm{Ro} = V_T/u$ (i.e., the ratio between the particles settling velocity and the fluid rms fluctuations). However, such behavior $(V_p - V_T)/u \sim -\mathrm{Ro}$ appears only to be valid for moderate values of the Rouse number.

DOI: 10.1103/PhysRevFluids.6.044305

I. INTRODUCTION

Turbulent particle-laden flows have a widespread presence in industrial and natural processes, e.g., coatings, spray combustion, pollen dispersion, planetesimal growth, and clouds' formation [1–3]. Among the several consequences of particle-turbulence interactions, preferential concentration and particle settling velocity modification have received considerable attention in the last decades [4–6]. Preferential concentration describes the tendency of particles to accumulate in space,

[*]Also at Department of Mechanical Engineering.
[†]martin.obligado@univ-grenoble-alpes.fr

forming clusters and voids. In contrast, particle settling modification accounts for the enhanced (respectively, hindering) of the particles' settling velocity in the direction of a body force acting on them, for instance, gravity.

Several theoretical approaches have suggested mechanisms that relate the topology of the background turbulent flow to the observed preferential concentration and settling modification. Regarding preferential concentration, classical contributions have suggested that *sub-Kolmogorov* particles, which have a characteristic scale smaller than the Kolmogorov scale η, tend to concentrate in regions of high strain and low vorticity [4,7]. However, recent research has proposed that this classical picture does not include the multiscale nature of turbulence. Under this framework, some studies have proposed that particles accumulate at the different (coarse-grained) scales of high strain and low vorticity [8]. Alternatively, other studies have shown evidence that particles mimic the clustering of the carrier phase zero acceleration points [9,10], which exhibits a self-similar behavior [11].

Regarding particles' settling modification, previous works have suggested that the modification of particles' settling velocity is due to centrifugal effects, a mechanism called preferential sweeping: inertial particles are expelled of eddies but fast-track into downward eddies, thereby enhancing their settling speed [7,12,13]. The opposite effect has also been observed: particles' settling velocity is reduced instead of being enhanced [14]. Some research has conjectured that this phenomenon occurs when particles preferentially sample the upward regions of the flow [14–16]. Recent research has also attempted to incorporate ideas from the multiscale nature of turbulence to understand the observed particle settling behavior. Some works argue that the centrifugal effect (and the enhanced settling) depends on the relationship between the particle inertia, and all of the carrier phase length scales, i.e., particles of different inertia are affected by different length scales of the turbulent flow [17].

Considering the complex interactions between the turbulent carrier phase, and the discrete particle phase, most studies treat preferential concentration and particle settling independently. Recent works [18–23], however, have aimed to relate both phenomena. For instance, some studies have reported that the enhanced particle settling is due to the increased local concentration (higher liquid fractions ϕ_v) [22,24]. In other words, particles in high-density regions settle (on average) faster with respect to particles in low-density regions [21–24].

Numerical and experimental studies do exhibit similar trends on the behavior of preferential concentration and settling velocity with global flow parameters, such as the Taylor-based Reynolds number $\mathrm{Re}_\lambda = u\lambda/\nu$ and the Stokes number $\mathrm{St} = \tau_p/\tau_\eta$, where u stands for the RMS value fluid fluctuating velocity u', λ corresponds to the Taylor microscale, ν is the kinematic viscosity, and τ_p and τ_η stand for the particle relaxation and the Kolmogorov timescales, respectively. Nevertheless, quantitative consensus between experiments and simulations has yet to be reached [17,20,23,25–27].

Moreover, the origin of these discrepancies could be multifold [20,25,28,29]. For example, the numerical and experimental study of Good *et al.* [29], at $\mathrm{Re}_\lambda \simeq 200$, and liquid fractions $\phi_v = 10^{-6}$ has shown that particle settling *hindering* effects cannot be captured in DNS simulations that only consider linear drag. Conversely, DNS simulations of Rosa *et al.* [28] report no variation in the particle settling velocity with the drag model, i.e., their results were insensitive to the choice of the drag law used (e.g., linear, nonlinear). Another source of discrepancy may stem from the mechanical coupling between particle phase and the turbulent carrier phase interaction, ignored in most DNS studies. The need to include these interphase mechanical coupling effects was recognized early by Aliseda *et al.* [24]. They suggested modifying the carrier phase pressure field to account for the flow regions with high particle density. Most DNS studies ignore this coupling and assume that the particles do not affect the carrier phase, a regime known as "one-way" coupling. Interestingly, Bosse *et al.* [25], and Monchaux *et al.* [20] observed a larger particle settling velocity when the mechanical coupling between the phases, a regime known as "two-way" coupling, was included. Their simulations, however, were run at rather small Reynolds numbers ($\mathrm{Re}_\lambda \approx 40$). A recent numerical study by Rosa *et al.* [30] has arrived at similar conclusions at higher Reynolds numbers

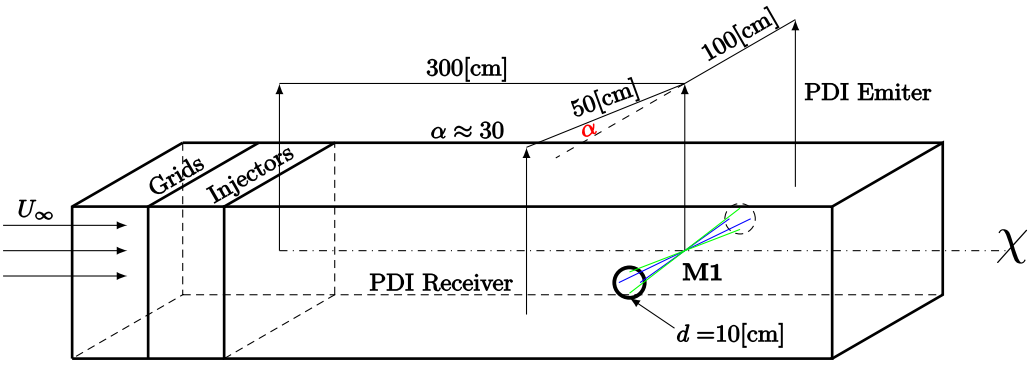

FIG. 1. Sketch of our experimental setup (not to scale). The wind-tunnel cross-section is $75 \times 75\,\mathrm{cm}^2$. Its center line is labeled as χ in the figure. The emitter and receiver components of the PDI are on the same horizontal plane. However, the receiver is positioned at 30 degrees (see α in the figure) with respect to the emitter to maximize the capture of the water droplets refraction [18,37]. Two holes of approximately 10 cm were carved onto the walls to counteract the water accumulation on them. The measuring station was located at the position labeled as **M1** on the wind-tunnel center line, and 3 m downstream of the droplets injection.

($\mathrm{Re}_\lambda \approx 100$). These findings hint that including two-way coupling interactions may be necessary to describe accurately the physics of the particles' settling modification.

In this work, we report experimental measurements of a polydisperse population of inertial particles settling under homogeneous isotropic turbulence downstream of an active grid. Considering that the impact of two-way coupling on the settling modification is yet to be dispelled, we run experiments at the smallest liquid fractions attainable, as previous research in our facility has shown that at liquid fractions $\phi_v = O(10^{-5})$ the particles' presence may affect the turbulence characteristics, [31] adding an extra layer of complexity. Thus, under these experimental conditions at $\mathrm{Re}_\lambda \in [230\text{–}650]$ and $\phi_v < O(10^{-5})$, our experimental results suggest that the Taylor-Reynolds number (Re_λ) is the leading contributor to the particles' behavior, influencing all the measurable regimes. For instance, the degree of hindering (i.e., the measured particle settling velocity is smaller than its respective value for still fluid conditions) increases with the value of Re_λ. Moreover, when we plot the settling velocity against the Rouse number, which is the ratio between the particles settling velocity and the fluid rms fluctuations $\mathrm{Ro} = V_T/u$, we find that the transition point between hindering and enhancement (i.e., particles falling faster than in a quiescent fluid) regimes shifts to smaller Rouse numbers at increasing values of Re_λ.

II. METHODS

A. Experimental setup details

The experiments were performed in a close-circuit wind tunnel "*Lespinard*" in the *Laboratoire des Écoulements Géophysiques et Industriels* (LEGI) at Université Grenoble Alpes. This facility has been regularly employed to study particle clustering under decaying *homogeneous isotropic turbulence* (HIT) conditions [3,32–34]. A sketch of our experimental setup is depicted in Fig. 1. We briefly explain our experimental setup, and the experimental methods used. In the experiments, the turbulent flow was generated utilizing an active grid [35] in triple random mode. We set our experiment following best practice guidelines. First, the active grid mesh size M is roughly a tenth of the tunnel width. As stated in previous studies on similar active grids and protocols (see Ref. [35] and references therein), within these conditions the mean velocity profile in both the vertical y and the spanwise z directions is expected to be fairly homogeneous. This ensures that at our measuring station, our Eulerian measurement is surrounded by a homogeneous box of size comparable to the integral lengthscale $\mathcal{L}$. As we focus on the homogeneous region of the flow, and in the dilute

TABLE I. Parameters of the unladen flow, measured by means of hot-wire anemometry, at the measuring station 3 m downstream of the grid. The parameters are defined as $u = \langle u' \rangle^{1/2}$, the turbulence energy dissipation rate $\varepsilon = 15\nu u^2/\lambda^2$, $\eta = (\nu^3/\varepsilon)^{1/4}$, and L is the integral length scale computed following [38]. The kinematic viscosity of the air is taken as $\nu = 1.5 \times 10^{-5}$ ($m^2 s^{-1}$). Finally, $\gamma = \varepsilon^{3/4}/(g\nu^{1/4})$ is the acceleration ratio.

Re_λ	U_∞ [ms^{-1}]	u/U_∞	L [cm]	ε [$m^2 s^{-3}$]	λ [cm]	η [μm]	γ
232	2	0.1273	5.70	0.0777	1.36	457	0.24
321	3	0.1343	7.21	0.2577	1.19	338	0.59
404	4	0.1405	8.45	0.6058	1.08	273	1.12
503	5	0.1476	9.80	1.1667	1.02	231	1.84
601	6	0.1541	11.10	2.1116	0.98	200	2.87
648	7	0.1578	11.58	3.3862	0.90	178	4.09

limit, we expect that particles will not have an impact of the background turbulent flow, particularly rendering negligible any effect that mean shear could have on the particles' behavior. Next, we measured the turbulent unladen velocity by hot-wire anemometry and computed the turbulent parameters using standard methods and assumptions (e.g., Taylor hypothesis). The most relevant unladen flow parameters are summarized in Table I. For detailed explanations on the turbulence characterization, see Ref. [36] and references therein. Figure 3(a) shows the unidimensional power spectral density spectra at the measuring station (see label "**M1**" in Fig. 1).

Second, downstream of the "grid" section (see Fig. 1) a rack of 18 or 36 spray nozzles—at smaller concentrations fewer injectors were used, see Fig. 2(a)—injected inertial water droplets with diameters D_p between 20 and 300 microns, i.e, $D_p \in [20\text{–}300]\,\mu$m. This polydispersity was characterized by phase Doppler interferometry and Spraytec granulometry [37]. The respective droplet distribution is close to a log-normal distribution [see fit in Fig. 2(b)]. Droplets were considered as spherical particles as their Weber number parameter was, for most droplets, below unity (see Sumbekova [39], Sec. 6.3). However, to have an adequate statistical convergence in our experimental realizations, we binned the measured droplets between 7.5 and 155 μm [see Fig. 2(c)].

Third, the measuring station was placed 3 m downstream of the droplet injection (see Fig. 1). The measuring volume lay at the centerline of the wind tunnel. We used a phase Doppler interferometry apparatus (PDI), model Artium-PDI-200, which can measure the settling velocity and the particles' diameter simultaneously [37,40]. The PDI setup has two components: the receiver and the laser emitter. The laser emitter was placed perpendicular to the gas flow. The receiver (see Fig. 1) was on the same horizontal plane but rotated 30 degrees to ensure adequate capture of spherical water droplets in the airflow.

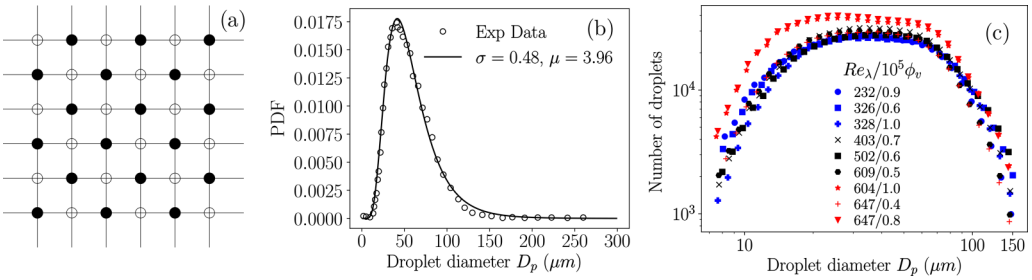

FIG. 2. (a) Injector rack sketch. For the lowest volume fractions half of the injectors (filled markers) were utilized. (b) Spray characterization coming from Spraytec data from Sumbekova [39]. (c) Droplet histogram obtained with the PDI for all experimental datasets reported in this work.

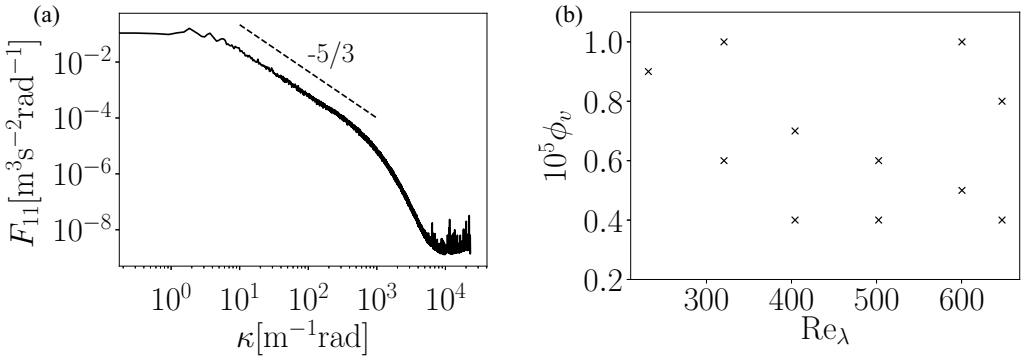

FIG. 3. (a) Example of an unidimensional power spectral density F_{11} [42] from one of our hot-wire records at measuring station **M1** (see Fig. 1). (b) Parameter space for the experiments conducted. The global liquid fraction was estimated as $\phi_v \approx Q_W/Q_A$, where Q_W and Q_A are the volumetric flux of water and air, respectively.

The PDI setup has two different laser beams (before splitting to form the fringes) that allow us to measure the two velocity components of the particles captured, and their respective diameter. Although it is desirable to have for each particle these three characteristics altogether (horizontal/vertical component, diameter), a compromise is required as coincident detection does significantly reduce the validation rate, i.e., the ratio between the number of particle events deemed as valid (a credible detection) over the total number of particle events. Hence, we set the PDI in noncoincident mode: the vertical velocity component and the particles' diameter were recorded by the largest wavelength beam (green laser in our case), whereas the streamwise velocity was recorded by the shortest wavelength beam (blue laser in our case). We made this choice to improve the validation rate (by a factor five or even larger). To quantify the effects of the carrier phase turbulence on the particles, we tried to match as close as possible, the particles' mean horizontal velocity ($\langle U_p \rangle$) to respective unladen mean velocity (U_∞), i.e., in our experiments $\langle U_p \rangle \approx U_\infty$. The validation rate reported by the PDI software was above 70% or higher in all experimental realizations. The acquisition rate (particles per second) varied between 400 and 3000 Hz depending on the liquid fraction and bulk velocity, i.e., a higher concentration at a higher bulk velocity yielded a higher acquisition rate. For each experimental condition, we collected data from 5×10^5 particles. The vertical (respectively, horizontal) velocity component had a resolution of 0.010 m/s (respectively, 0.04 m/s) for all experimental conditions.

Finally, it is worth nothing that the choice of the measurement position (3m downstream of the injection) was based on previous studies in the same facility. These studies report that at 3m downstream of the injection, the particle velocity statistics are almost Gaussian (see in Appendix A, Figs. 11(a)–11(b)), meaning that the particles' velocities have relaxed to the background fluid fluctuations. Hence, our measurements are able to gauge the effects of the background turbulence on the particle behavior. However, and as mentioned in the introduction, a recent study in our facility reports that the carrier phase turbulence may change due to the particles presence [31]. To curb the influence of such turbulence modulation due to the particles' presence, we ran the experiments with the smallest liquid fractions attainable in our facility [39] (i.e., $\phi_v = [10^{-6}, 10^{-5}]$). We expect that, at these liquid fractions, the turbulence modulation is strongly reduced [41]. Altogether, these previous considerations led to the exploration of a parameter space aiming to small concentrations and large Reynolds numbers, exploiting the limits of the experimental facility (see Fig. 3(b)).

B. Velocity measurements and angle correction

There will always be a small deviation angle between the PDI axes and the wind tunnel coordinate system (see Fig. 4) impacting the vertical velocity measurements. Considering that the

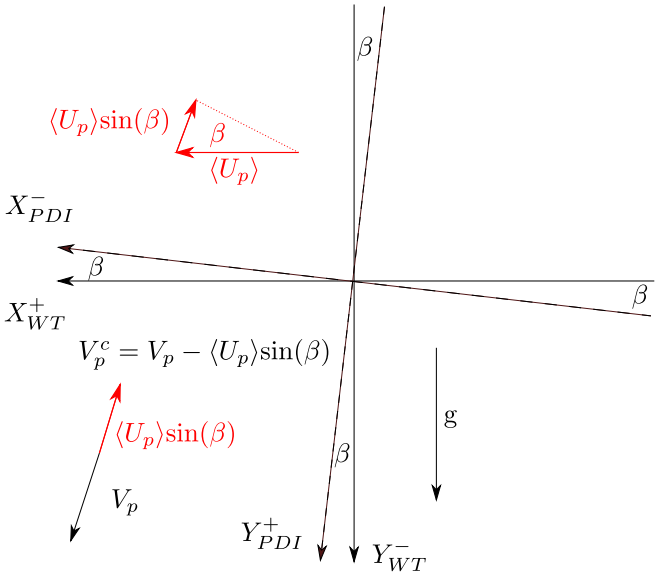

FIG. 4. Coordinate systems for the wind tunnel and the PDI device.

particles' horizontal velocity is at least an order of magnitude larger than the vertical one, the horizontal component's projection onto the vertical component in the PDI coordinate system will cause an error in the vertical velocity measurements due to such optical misalignment. We address this problem by subtracting the projected mean droplet horizontal ($\langle U_p\rangle$) velocity from the vertical velocity in the PDI coordinate system (V_p). We define this angle-corrected velocity as

$$V_p^c = V_p - \langle U_p\rangle\sin(\beta) = V_p - V_\beta, \quad V_\beta = \langle U_p\rangle\sin(\beta). \tag{1}$$

To calculate V_β, we used a different configuration in the wind tunnel. We used a single particle injector, positioned at the grid plane and set the grid completely open, thus minimizing turbulence. We circulated air at 3.5 ms^{-1} and injected olive oil droplets, with a very narrow distribution of sizes, centered around a mean diameter $\approx 8\,\mu$m (measured with the PDI). Olive oil droplets were convected downstream of grid by the bulk flow, and we recorded droplets' velocities at the PDI measuring volume (see Fig. 1). The velocity statistics collected for 2000 droplets in the PDI frame of reference (see Fig. 4) were $\langle U_p\rangle = (-3.52 \pm 0.02)$ m/s, $\sigma_{U_p} = (0.11 \pm 0.02)$ m/s, and $\langle V_p\rangle = (-0.09 \pm 0.005)$ m/s, $\sigma_{V_p} = (0.11 \pm 0.005)$ m/s. Then, we estimated the expected settling velocity of droplets via the Schiller and Nauman [43] drag coefficient semiempirical formula. Our experimental values, the Schiller and Nauman formula and our resolution yielded a correction angle $\beta = -1.5^\circ \pm 0.3^\circ$ (the angle uncertainty is fruit of the PDI velocity resolution), which we used for all experimental realizations. This optical alignment correction for all particles is justified under our turbulent conditions because this correction is smaller than the standard deviation of the carrier phase velocity, i.e., $V_\beta/u = \sin(\beta) \times \langle U_p\rangle/u \approx \sin(1.5^\circ) \times O(10) < 1$ (see Table I and Fig. 11).

III. MEASUREMENTS

A. Raw settling velocity

We will consider the particles' vertical velocity to be positive toward gravity in agreement with the PDI coordinate system (Fig. 4). We binned our datasets by the droplet diameters [see Fig. 2(c)]. The amount of droplets per bin follows the droplet size distribution PDF [Fig. 2(b)]. These bins had a size of 5 μm (an operation represented by $\langle\rangle|_D$) and their centers spanned $D_p \in [7.5\text{–}155]\,\mu$m. This latter consideration is due to the injector droplet size distribution and has some consequences:

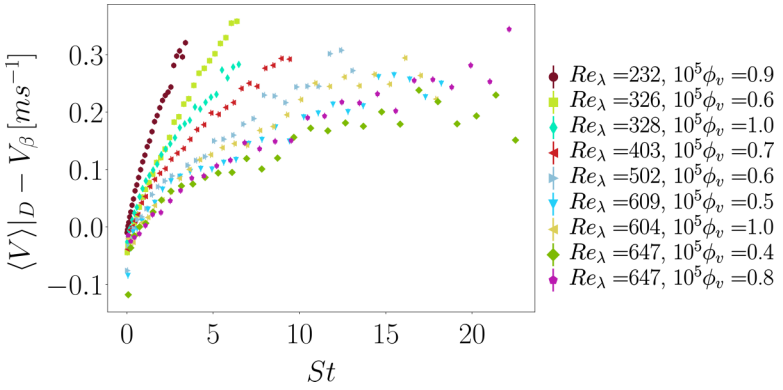

FIG. 5. Particle vertical velocity measurements binned by diameter size against the binned Stokes number. Error bars have a size $\pm 5 \times 10^{-3}$ ms^{-1} (half of the PDI resolution).

smaller droplets are less common [see Fig. 2(b) for an example of size distribution], and therefore, our first bins have a larger variation. We, nevertheless, collected enough samples to have meaningful statistics. For instance, in Fig. 2(c), we show that each bin had at least 1000 particles.

The polydispersity of our droplet injection and our active grid turbulence characteristics (e.g., higher values of ε, see Table I) allows to explore a wide range of particle Stokes numbers for the different experimental conditions (see Fig. 5). Interestingly, for all particle sizes, the particles' velocities decrease with increasing Re$_\lambda$ (i.e., slower settling in our convention). Moreover, our raw velocity measurements show that for a fixed experimental condition particles with larger Stokes (larger diameters in our case) fall—on average—faster (see Fig. 5), as expected. However, there are two sources of uncertainty in our results for the smallest droplets: first, the accuracy of the optical alignment, and second, the vertical resolution used (0.010 m/s). This vertical resolution results from a tradeoff between an adequate acquisition rate and the statistical convergence needed.

In this work, we refrained from analyzing the preferential concentration from 1D particle records, for instance via 1D Voronoï tessellations [44], as a previous work from the group suggests that these statistics in our experimental setup may present biases that could lead to misleading conclusions see Ref. [45]. Nonetheless, the presence of clusters (higher density regions with respect to the average concentration) and voids (lower density regions with respect to the average concentration) may be of relevance in this problem. Particularly considering the polydispersity of injected droplets. For instance, while particles belonging to clusters and voids tend to have different settling velocities than the particles not belonging to any of them [22], the droplet size distribution within these structures can be significantly different from the size distribution at the droplet injection station. While we cannot measure this phenomenon with our experimental setup, it may play an important role and further research is needed. In our experiments, to curb the influence of clusters and voids, we deliberately ran experiments at the lowest of ϕ_v attainable, aiming to reduce the influence of these collective effects in our measurements.

B. Settling parameters, and nondimensional numbers

The turbulent carrier phase is usually characterized by the Taylor Reynolds number $\mathrm{Re}_\lambda = u\lambda/\nu$. There is still an open debate (see Ref. [39] and references therein) about which parameters are adequate to describe the dynamics of the discrete phase. For instance, in the literature, the impact of the Stokes, Rouse, Reynolds, and Froude numbers [defined below through Eqs. (2)–(6)] on the settling velocity have indeed been reported but there is no consensus on the governing scaling laws. Our aim is to disentangle (within the limitations of our experimental setup) the independent influence of these parameters. For example, the role of the Stokes number is well known to control

preferential sweeping (or fast track, see Maxey [7]). However, for droplets with a high settling velocity (high Rouse number), the settling speed is expected to be modified by loitering (Nielsen [14]) and, hence, it should be controlled by the ratio of fluid to gravity accelerations (a Froude number). In fact, a global nondimensional analysis (detailed in Sec. 6.5 of Ref. [39]) yields that the nondimensional settling velocity is expected to depend on five independent parameters: the local volume fraction, the particle to fluid density ratio, the turbulent Reynolds number, the Stokes number, and the Rouse number.

The Froude number could be used in lieu of the Stokes or of the Rouse number as there is an exact relationship between Fr, Re_λ, St, and Ro [see Eqs. (5) and (6)]. In our experiments, we note that the particle to fluid density ratio is very large so that we can consider that the system is within its asymptotic regime with respect to that parameter. As we kept the volume fraction very low (ideally low enough to avoid turbulence modulation), it can be argued (subject to *a posteriori* verification) that the system is also in an asymptotic regime with respect to the volume fraction. Therefore, we are left with three "independent" parameters: Re_λ, St, and Ro, any of which can be exchanged by the Froude number. Then, inspection of definitions Eqs. (5) and (6) suggests that relationships can be constructed for any combination of Rouse, Froude, Reynolds, or Stokes numbers. However, among the possible experimental parameters, below we present results using the combination Ro, Re_λ, and St. Although we do not argue that this parameter space combination is complete, it is supported by our experiments as well as the experiments we found in the literature. Indeed, for ours and previous experimental data plotted under this set of parameters, a key observation is that the settling velocity at large Rouse number is controlled to first order by the fluid velocity fluctuations (represented by the Reynolds number) and not by fluctuations in the fluid acceleration, as we may have expected in the loitering scenario.

Considering the previous discussion, we proceed to define the most common nondimensional numbers used to analyze the particles settling velocity. Classical numerical and experimental studies [13,24] plot the particles settling velocity against the Stokes number $\mathrm{St} = \tau_p/\tau_\eta$ (see Fig. 5); changes in the turbulence dissipation lead to changes in the Stokes number. Other nondimensional parameters of interest involve the ratio between the particle terminal speed (V_T) and the background turbulence rms fluctuation, known as the Rouse number, $\mathrm{Ro} = V_T/u$ [20,39] (some authors also refer to this nondimensional number as the settling parameter Sv [23,29]). Algebraic manipulations allow combining both Rouse and Stokes numbers as follows:

$$\mathrm{St} = \frac{\tau_p}{\tau_\eta} \rightarrow \mathrm{St} = \frac{\tau_p}{\tau_\eta}\frac{u}{u}\frac{g}{g} \rightarrow \mathrm{St} = \mathrm{Ro}\frac{u}{\tau_\eta g}. \tag{2}$$

The particle relaxation time includes the nonlinear drag from Schiller and Nauman [43],

$$\tau_p = \frac{\rho_p D_p^2}{18\mu_f\left(1 + 0.15\mathrm{Re}_p^{0.687}\right)}, \quad V_T = \tau_p g, \tag{3}$$

where g stands for earth's gravitational acceleration, μ_f is the fluid viscosity, Re_p is the particle Reynolds number, and ρ_p the particles density (water). In addition to St and Ro, some research suggest that the ratio between the turbulent acceleration (η/τ_η^2) and gravity may play a role on the results. Some authors refer to this ratio as $\gamma = \eta/(g\tau_\eta^2)$ [14,22,29], while others refer to it as a *Froude* number [17,46] (Fr). In this work, we will follow the former notation. From Eqs. (2)–(4), and taking into account that $\lambda = \sqrt{15}\tau_\eta u$ (small scale isotropy), one gets

$$\gamma = \frac{\varepsilon^{3/4}}{g\nu^{1/4}} = \frac{\eta}{\tau_\eta^2 g}, \tag{4}$$

$$\mathrm{St} = \gamma\frac{\mathrm{Ro}\mathrm{Re}_\lambda^{1/2}}{15^{1/4}}, \tag{5}$$

$$\mathrm{Ro} = 15^{1/4}\frac{\mathrm{St}}{\gamma \mathrm{Re}_\lambda^{1/2}}. \tag{6}$$

Moreover, combinations of these parameters such as RoSt (involving the Rouse and Stokes numbers) have recently received some attention, as they appear to give a better collapse of the data [12,23,29]. For instance, for the RoSt, one gets from Eqs. (5) and (6) that

$$\mathrm{RoSt} = \frac{V_T}{u}\frac{\tau_p}{\tau_\eta} \sim V_T\frac{\tau_p}{\lambda}, \tag{7}$$

which seems to take into account the influence of the background turbulence on the particle settling velocity; the ratio between the particle stopping distance to the Taylor microscale λ, which scales with the average distance between velocity stagnation points [36,47–50].

In our experiments, we cannot change the magnitude of the acceleration of gravity (g) or the magnitude of the air kinematic viscosity (ν). As a result, we cannot easily disentangle or individually vary, Ro, St, and γ. Actually, we can only increase the turbulence dissipation ε (and the absolute magnitude of the turbulence RMS fluctuations) by increasing the inlet velocity U_∞. These constraints yield similar functional behaviors for γ, and Re_λ. To overcome these restrictions and acquire a broader understanding of the physical phenomena at play, we compare our results with other experimental datasets taken from different experimental studies.

C. Normalized settling velocity

To quantify the degree of settling enhancement, we compute the velocity difference between the particle settling velocity and its terminal speed $\Delta V = \langle V\rangle|_D - V_T - V_\beta$, where V_β includes the misalignment effects. ΔV is usually normalized by the carrier phase fluctuations u, or by the particle terminal speed V_T [4,13,18,23,24,28,46]. Interestingly, previous experiments [18,29], as well as ours, reveal that the particle velocity is hindered (slowed down with respect to the still fluid terminal velocity) as the Re_λ increases above a certain threshold (see Fig. 6). Other experiments, e.g., Akutina *et al.* [51] have also reported hindering for particles falling inside a turbulent column. Although particles with small Rouse and Stokes numbers have settling velocities (magnitudes) that depend strongly on the liquid fraction ϕ_v and Re_λ, we observe that for $\mathrm{Ro} > O(0.1)$ (after the peak of maximum settling enhancement) the normalized particle settling ($\Delta V/u$) seems to have a quasilinear behavior (see Fig. 6). To the best of the authors' knowledge, this regime is not predicted by any available analytical model. We also observe that hindering is present at large St number when $\Delta V/u$ is plotted against the Stokes number. The latter observations imply each other due to the relationship between Rouse and Stokes numbers [cf. Eq. (5)].

We note that our data exhibits hindering effects at very small St, and Rouse numbers, in agreement with findings in other experimental facilities, e.g., experiments in grid tanks [52] and in a turbulence box [23]. However, we must note that these conclusions require further research given the difficulty of recovering the "tracer" behavior in similar experimental measurements, i.e., a particle that almost perfectly follows a fluid parcel. To recover this behavior using laser interferometry (e.g., PDI) and imaging (e.g., PIV, PTV), it is required that the optical alignment is very accurate so that the absolute zero is adequately set. Besides proper alignment, we also need two extra elements: very dilute conditions $\phi_v \to 0$, and, in our specific case, very small particles $\mathrm{St} \to 0$. Thus, it is not surprising that most experiments have reported values of $\Delta V \neq 0$ for $\mathrm{St} \to 0$ [18,29,53]. It is worth noting that we included some previous experimental data at higher liquid fractions than our experiments $\phi_v > 1 \times 10^{-5}$ from the experiment of Aliseda *et al.* [24]. Although at these higher concentrations the mechanical coupling between phases (two-way coupling) may start to play a role into the settling velocity, all trends with respect to the Rouse and Reynolds numbers seem to be consistent with our results in the dilute regime. As discussed by Aliseda *et al.* [24], for those

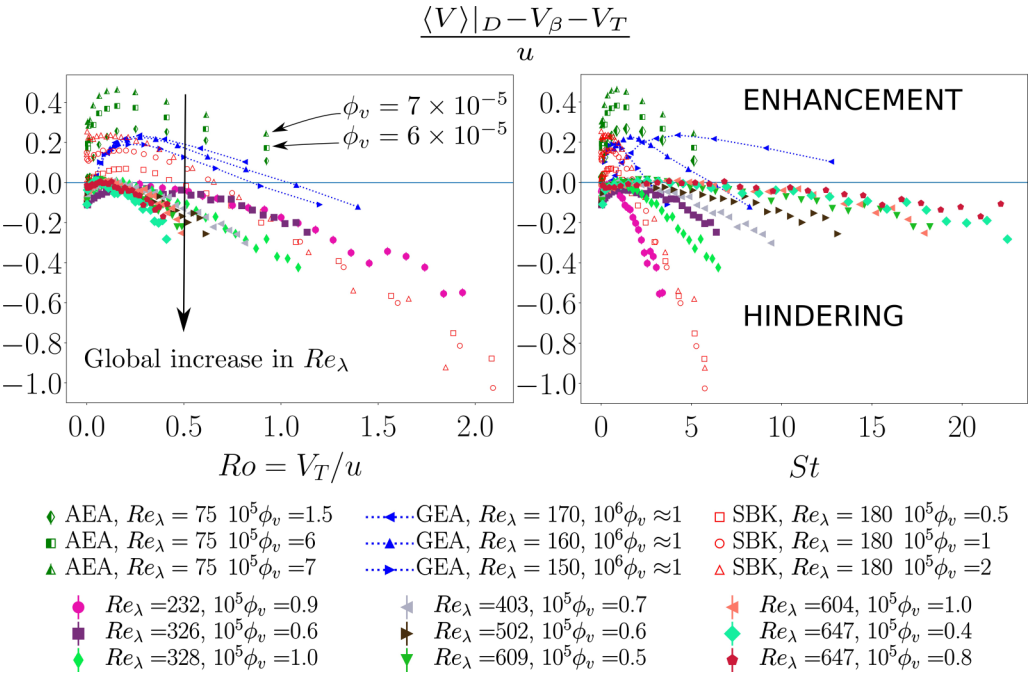

FIG. 6. Particle velocity over the carrier phase fluctuations against Rouse (left) and Stokes numbers (right). In the figures legend GEA refers to the data of Good *et al.* [29]. AEA refers to the data of Aliseda *et al.* [24], and SBK refers to the data of Sumbekova [18]. Error-bars denote the resolution uncertainty, and they are masked by the size of the markers on the plot.

experimental datasets, the higher concentration seems to induce an upwards shift in the settling velocity. We will revisit the effects of concentration in our results in the next Sec. IV B.

Moreover, our measurement resolution could also have an impact on the measurements taken in the low St regime. These resolution limitations can be clearly observed when the velocity ΔV is normalized against V_T (in the Appendix B 1 see Figs. 12(a), and 12(b) and the large error bars for small Rouse). We also note that these conclusions could be biased by a condition that may exist due to the spatial domain where the experiments take place (confinement effects): weak recirculation currents that perturb the settling dynamics of the particles. These perturbations could be of the order of the settling velocity for small inertial particles biasing the results measured. These biases imply that the tracer behavior may not be recovered, $\Delta V/V_T \neq 0$ for $\mathrm{St} \to 0$, and therefore, measuring the true values of $\Delta V/V_T$ for $\mathrm{Ro} \ll 1$ or $\mathrm{St} \ll 1$ is not straightforward.

For instance, Good *et al.* [53] reports $\Delta V/V_T \to O(100)$ for $\mathrm{Ro} \ll 1$ in wind tunnel experiments, but in a following publication, Good *et al.* [29] suggest their previous experimental observation (i.e. $\Delta V/V_T \geqslant O(10)$ for $\mathrm{Ro} \ll 1$) was due to a weak mean flow. Likewise, Akutina *et al.* [51] reports a similar phenomenon in grid-tank experiments: "The intensity of these mean fluid motions can be of the order of the particle settling velocity and therefore strongly affects the measurements."

Given the difficulty of measuring both phases simultaneously at our values of Re_λ, we are unable to asses the impact of these recirculation cells on our results. Future research should address the impact of these weak mean flows on the small Rouse regime. To circumvent these nonzero vertical mean flow effects, we suggest in Sec. V to analyze the droplets' settling in a translating frame of reference. Considering these experimental difficulties found in the double limit of $\phi_v \to 0$, and $\mathrm{St} \to 0$, we will focus our analysis on bulk trends of the moderate Rouse regime, which is less sensitive to these measuring uncertainties.

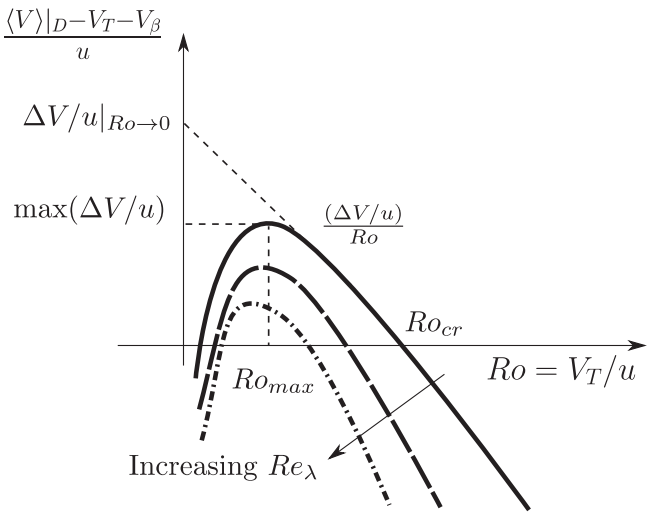

FIG. 7. Parameters computed from the data in Fig. 6 . The different line styles refer to different values of Re$_\lambda$.

IV. MODERATE ROUSE REGIME

A. Global behavior

We focus on the regime Ro $> O(0.1)$, and analyze the particles velocity settling curves against the Rouse number (see Fig. 7). The curve is defined by its slope, x-axis intercept (crossover between hindering and enhancement) and its maximum. For those datasets that have not reached hindering, we extrapolated the crossover with a linear fit. First, we consider the scaling of Sumbekova *et al.* [18] for a similar range of Rouse numbers (other scalings proposed for this regime are included in Appendix B 2). They propose that the crossover Ro$_{cr}$, which defines the boundary between hindering and enhancement, increases with $\gamma_a = a_0^{1/2}\gamma$, where $a_0 = 0.13\mathrm{Re}_\lambda^{0.64}$ is the Lagrangian acceleration correlation proposed by Sawford [54]. This proposal seems to hold to some extent for previous datasets [see Fig. 8(a)] but it does not hold for our data (black markers), which seems to be less affected (if at all) by variations of the fluid acceleration. For the sake of completeness, we also plotted our data using different scalings found in the literature (see Appendix B 2). Interestingly, our data reveal that Ro$_{cr}$ [Fig. 8(b)] becomes smaller with increasing Re$_\lambda$, in agreement with [16,53]. Although the liquid fraction does impact Ro$_{cr}$, the leading order contribution comes from Re$_\lambda$. It is then left for future research to assess whether these effects could be facility dependent (e.g., due to a non-zero mean vertical flow [29,39,51]).

The linear fit y intercepts (i.e. the limit Ro $\to$ 0 in Table II) also decrease with increasing Re$_\lambda$. This trend is consistent with the observed reduced settling at increasing Re$_\lambda$ (Fig. 7). However, the fitted linear slopes [Fig. 8(c)] are of order 1, i.e., $(\Delta V/u)/\mathrm{Ro} = \Delta V/V_T = O(1)$, and they seem to become steeper with Re$_\lambda$. The correlation with Re$_\lambda$, however, is not conclusive, as multiple factors (e.g., recirculation cells, and volume fraction ϕ_v) could be influencing the results. Interestingly, this quasilinear behavior has also been recovered in numerical simulations, where the horizontal motion of the particles was suppressed [28].

The maximum settling enhancement [Fig. 8(d)] also decreases with Re$_\lambda$ in agreement with [19]. Likewise, the Rouse number corresponding to the peak enhancement of the settling velocity decreases with Re$_\lambda$ [Fig. 8(d)]. This observation may be a direct consequence of the coupling between u and Re$_\lambda$ in our experiment: they both scale with the inlet velocity U_∞. Thus, Ro $= V_T/u$ decreases with increasing Re$_\lambda$. These characteristics of ΔV vs Ro are summarized in Table II.

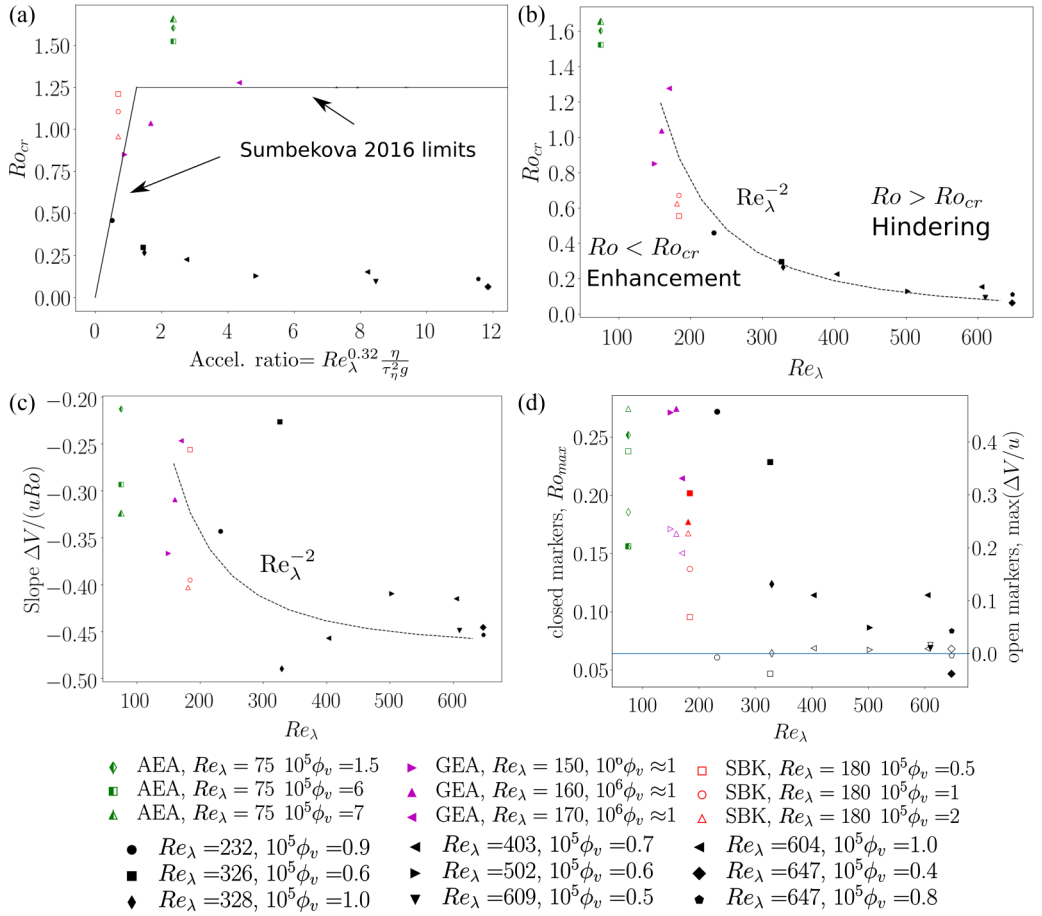

FIG. 8. (a) Ro_{cr} cross over between enhancement and hindering against $\gamma_a = \sqrt{0.13 Re_\lambda^{0.64}}\gamma$. The solid lines refer to the proposed scaling in Ref. [39]. (b) Ro_{cr}: crossover value between enhancement and hindering against Re_λ. (c) Slope of the settling velocity against Rouse number $(\Delta V/u)/Ro$. (d) Maximum settling velocity, and Rouse value for these maxima.

B. Local concentration effects

Some experimental studies report that the increased local concentration has an impact on the particle settling velocity due to preferential concentration [22,24], a mechanism frequently referred to as *collective effects*. In the same facility, previous research has found, utilizing 2D images, evidence of preferential concentration under similar experimental conditions as those studied here [3]. Based on the approach of Ref. [55], we decided to normalize ΔV by the cluster velocity $V_{cl} \sim \langle C_{\rm cl}\rangle \langle A_{\rm cl}\rangle \rho_p g/(\rho_{\rm air}\nu)$, where ρ_p is the particle density, $\langle C_{\rm cl}\rangle$, and $\langle A_{\rm cl}\rangle$ are the clusters concentration, and area, respectively. We estimate the latter quantities as $\langle C_{\rm cl}\rangle \approx 4\phi_v$ from 2D correlations in the same facility [3,22,32], and $\langle A_{\rm cl}\rangle = 2.1 \times 10^{-5} {\rm St}_{\rm max}^{-0.25} {\rm Re}_\lambda^{4.7} \phi_v^{1.2}$ [3]. The mean concentration range has also been reported for anisotropic turbulence [56] at mass loadings between 1% to 7%.

The normalization by a single velocity scale fails to account for the different trends observed (Fig. 9(a)). Tom and Bragg [17] claimed that normalizing the settling velocity results with a single length scale (or velocity scale) may not be adequate due to the multiscale nature of the turbulence. They advance that the particle settling is affected by the multiscale phenomenology of turbulent flows, and the resulting particle settling is due to an integrated effect of a range of scales that depend

TABLE II. Summary of the parameters extracted from Figs. 8(a)–8(d).

	$10^5\phi_v$	Re_λ	γ	ε	η	Slope	$\Delta V/u\|_{Ro\to 0}$	Ro_{cr}	Ro_{max}	$max(\Delta V/u)$
AEA 1	1.5	75	1.630	1.000	241	−0.213	0.341	1.602	0.252	0.267
AEA 2	6.0	75	1.630	1.000	241	−0.293	0.446	1.523	0.156	0.382
AEA 3	7.0	75	1.630	1.000	241	−0.324	0.536	1.657	0.156	0.463
GEA E1	0.1	150	0.500	0.200	360	−0.367	0.312	0.851	0.215	0.190
GEA E2	0.1	160	0.900	0.460	290	−0.309	0.321	1.037	0.274	0.227
GEA E3	0.1	170	2.300	1.600	220	−0.247	0.315	1.277	0.271	0.236
SBK 1	0.5	185	0.490	0.200	400	−0.256	0.310	0.555	0.202	0.069
SBK 2	1.0	185	0.490	0.200	400	−0.395	0.436	0.671	0.202	0.160
SBK 3	2.0	185	0.490	0.200	400	−0.405	0.386	0.624	0.177	0.227
This study	0.9	232	0.243	0.078	455	−0.343	0.157	0.459	0.272	−0.007
This study	0.6	326	0.625	0.277	332	−0.226	0.067	0.297	0.229	−0.038
This study	1.0	329	0.641	0.286	330	−0.490	0.130	0.266	0.124	0.001
This study	0.7	403	1.118	0.601	274	−0.457	0.104	0.227	0.114	0.010
This study	0.6	503	1.840	1.168	232	−0.410	0.052	0.128	0.086	0.007
This study	0.5	610	3.014	2.255	197	−0.449	0.042	0.094	0.069	0.016
This study	1.0	605	2.934	2.176	198	−0.415	0.064	0.153	0.114	0.009
This study	0.4	647	4.141	3.444	177	−0.445	0.028	0.063	0.047	0.009
This study	0.8	648	4.040	3.333	178	−0.454	0.050	0.110	0.083	−0.004

on the particle Stokes number. They argue that some physics may be lost by using a single scale to normalize the particle settling velocity enhancement, and therefore, the better collapse of the data brought by the use of the mixed length scales normalizations (Kolmogorov-scale velocity scaling combined by integral-scale Stokes [29]) is an indication of the multiscale nature of particle settling. Consistent with their observations, we see a slightly better collapse when using mixed scalings (viscous and integral scales combined) (see Fig. 9(b)).

V. ANALYSIS ON A MOVING FRAME OF REFERENCE

As stated in Sec. III C, nonzero mean vertical flow effects could potentially impact the results presented here. To address these biases, we conduct a final analysis considering the particle settling velocity in a frame of reference moving with the particle distribution global average;

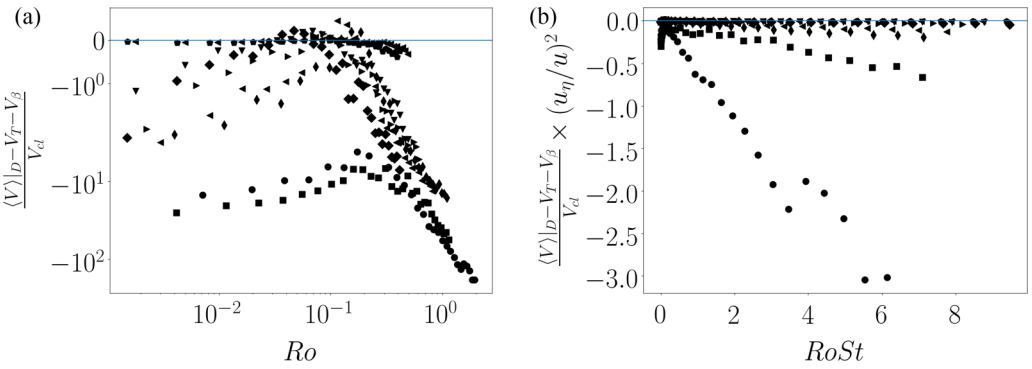

FIG. 9. Settling velocity normalized by different scales including the estimated settling velocity V_{cl} following the approach of Obligado *et al.* [55]. The vertical axis in panels (a) and (b) is negative log, i.e., $-1 \times$ log. The black markers follow the legend found in Fig. 8

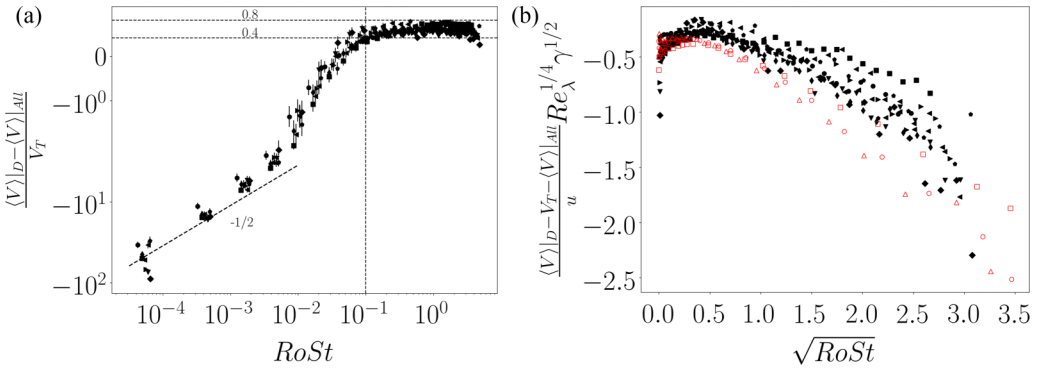

FIG. 10. (a) Settling velocity in a relative frame. Error bars account for the velocity vertical resolution ± 0.005 ms^{-1}. (b) Scaling of Eq. (10) applied in the relative moving frame of reference. Black markers represent our experimental data, red hollow markers are data of Sumbekova [18]. The legend follows Fig. 8.

$\langle V\rangle|_{\text{all}} = \int V(D_p) f(D_p) dD_p$, where $f(D_p)$ is the particle distribution PDF [see Fig. 2(b)]. In this moving frame of reference, we encounter the following question: *Which parameter does control the evolution of the particle in the translating frame of reference?* After some iteration, we find that the scaling RoSt, combining the Rouse and the Stokes numbers [see Eq. (7)], provides the best collapse of the data (see Fig. 10(a)) in the x coordinate that Ro or St individually.

Interestingly, in the regime RoSt > 0.1, the relative particle settling velocity has a slow evolution (see Fig. 10(a)):

$$\frac{\langle V\rangle|_D - \langle V\rangle|_{\text{all}}}{V_T} \approx C, \tag{8}$$

with $C \in [0.4\text{–}0.5]$, which after algebraic manipulation gives

$$\frac{\langle V\rangle|_D - \langle V\rangle|_{\text{all}} - V_T}{u} \approx (C-1)\text{Ro}. \tag{9}$$

This expression is consistent with the quasilinear behavior found in Fig. 6. Although the datasets present some variability at small Rouse numbers, we observe a power-law dependency for small RoSt $\ll 10^{-2}$. If we were to apply this observed power law, then algebraic manipulations would yield

$$\frac{\langle V\rangle|_D - V_T - \langle V\rangle|_{\text{all}}}{u} \approx C_\dagger \left(\frac{15^{1/4}}{\gamma \text{Re}_\lambda^{1/2}}\right)^{1/2} - \text{Ro}. \tag{10}$$

This result suggests that at very small Rouse numbers it would be possible to bound these profiles within the values of parameter $C_\dagger$. The data has a better collapse in this framework when multiplied by the mixed scaling (see Fig. 10(b)). The effects of $\langle V\rangle|_{\text{all}}$ and its relationship with the particle size distribution and the observed particle settling should be further investigated in future experiments. For instance, some experiments have advanced that a bidisperse particle distribution may fall faster than any of the two monodisperse ones [57], an enhancement that cannot be explained by simple linear superposition, i.e., by taking an effective diameter of the bidisperse distribution.

VI. CONCLUDING REMARKS

Using phase Doppler interferometry, we experimentally investigate the behavior of polydispersed inertial sub-Kolmogorov particles under homogeneous isotropic turbulence for turbulent Reynolds

numbers up to ≈ 650. Combined with previously available experimental results in the range $Re_\lambda \in [75–200]$ taken in different facilities [18,24,29], we find that the average settling velocity of particles is mainly a function of the Rouse number of the particle (Ro) and the overall particle-turbulence interactions are governed by the Taylor Reynolds number (Re_λ). We are unable to recover any strong influence from other parameters such as the ratio between the rms acceleration and gravity (γ) on the particle settling behavior.

Our results also suggest that at increasing values of Re_λ, the particles settling velocity is more hindered: their measured particle settling velocity is smaller than their respective one in still fluid conditions. This observation is recovered when the droplets' settling velocity is plotted against the Rouse numbers for each experimental condition explored.

A close inspection of the difference between the measured particle settling velocity and their respective one in still fluid conditions reveals that the boundary between the particle settling hindering ($\Delta V/V_T < 1$) and enhancement ($\Delta V/V_T > 1$) regimes also depends on Re_λ. The onset of such transition point seems to behave as Re_λ^{-2}. In addition, we find that after the peak of enhancement $\Delta V/u' \approx -\kappa \mathrm{Ro}$ decreases almost linearly with the Rouse number. This behavior starts in the enhancement region and goes well into the hindering region for all the Rouse numbers considered $\mathrm{Ro} < 10$. Noteworthy, the κ parameter, which accounts for this linear behavior, seems also to be a function of Re_λ for a fixed particle distribution: the larger the Re_λ, the steeper the decrease.

Although our concentration range is narrow to reach a definite conclusion, we do not recover a strong influence of the concentration on the results presented. This lack of influence seems to be a consequence of the more dilute conditions of our experiments ($\phi_v \leqslant O(10)^{-5}$) with respect to those conducted in the same facility [3], which report the existence of preferential concentration. Previous studies [22,24] have shown that the existence of preferential concentration leads to enhanced settling velocity for those particles inside a clusters. Sumbekova *et al.* [3] reports that the degree of clustering, as well as the clusters' characteristic size is an increasing function of Re_λ. On the contrary, we conjecture that these *collective effects* [22] become less important at increasing values of Re_λ where the hindering effect takes control of this phenomenon. 2D PTV measurements taken in the same facility support such conjecture: [19] reports that for a fixed droplet distribution, increasing Re_λ leads to a global reduction in the measured particle settling velocity for particles inside clusters.

Finally, we cannot rule out that our wind tunnel experiments might be affected by a nonzero mean vertical velocity, as proposed by previous research [29,39]. To address this potential bias, we have plotted our data in a translating frame of reference moving at the mean vertical velocity of our particle distribution. Previous experimental data as well as ours seem to collapse better in this frame, and it aids in explaining the quasilinear behavior in the absolute (laboratory) frame of reference past the peak of enhancement.

ACKNOWLEDGMENTS

Our work has been partially supported by the LabEx Tec21 (Investissements d'Avenir Grant Agreement No. ANR-11-LABX-0030), and by ANR Project No. ANR-15-IDEX-02. We also thank L. Vignal and V. Govart for their help with the experiments.

APPENDIX A: PARTICLE VELOCITY PDFs

Particle velocity PDFs (see Figs. 11(a)–11(b)) supporting the claim of Gaussian statistics made on Sec. II A.

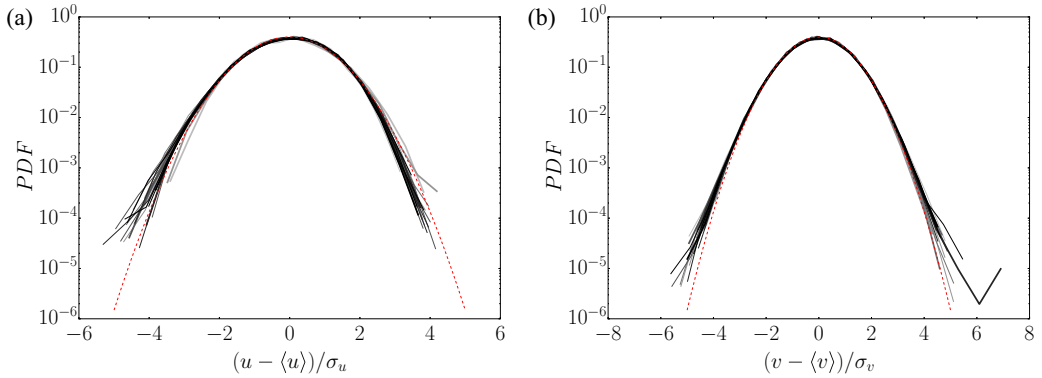

FIG. 11. PDFs of the particles velocity for the different records. (a) Horizontal component. (b) Vertical component. The darker the color the larger Re_λ. In the figures, the normal distribution is plotted as a dashed line (- - -).

APPENDIX B: ALTERNATIVE SCALINGS

1. Normalization by V_T

If the particles datasets were to be normalized by the respective terminal velocity, then we obtain the results found in Figs. 12(a) and 12(b).

2. Sumbekova *et al.* [18]

The scaling of Sumbekova *et al.* [18] (Fig. 13(a)) does not show a better collapse when compared to those we include in the main text. In the figure, some of the curves look closer, but this could be an effect of the y scale used. However, when large and small fluid scales are are combined with the cluster falling velocity the curves come close together to some extent (Fig. 13(b)). This highlights again that including multiple scales may be necessary to understand the underlying physics of the particle settling modification by the turbulent carrier phase.

Rosa *et al.* [28] also found a linear hindering behavior, consistent with our findings of Sec. IV A, with a slope close to -0.3, when the lateral movement of the particles was suppressed in direct numerical simulations (Fig. 13(c)).

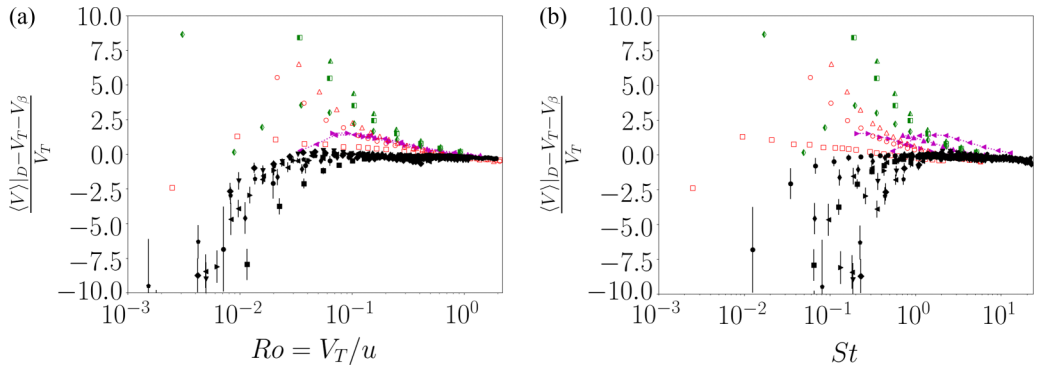

FIG. 12. Particle velocity over the particle terminal speed. (a) Against Rouse. (b) Against stokes. The markers follow the legend of Fig. 8.

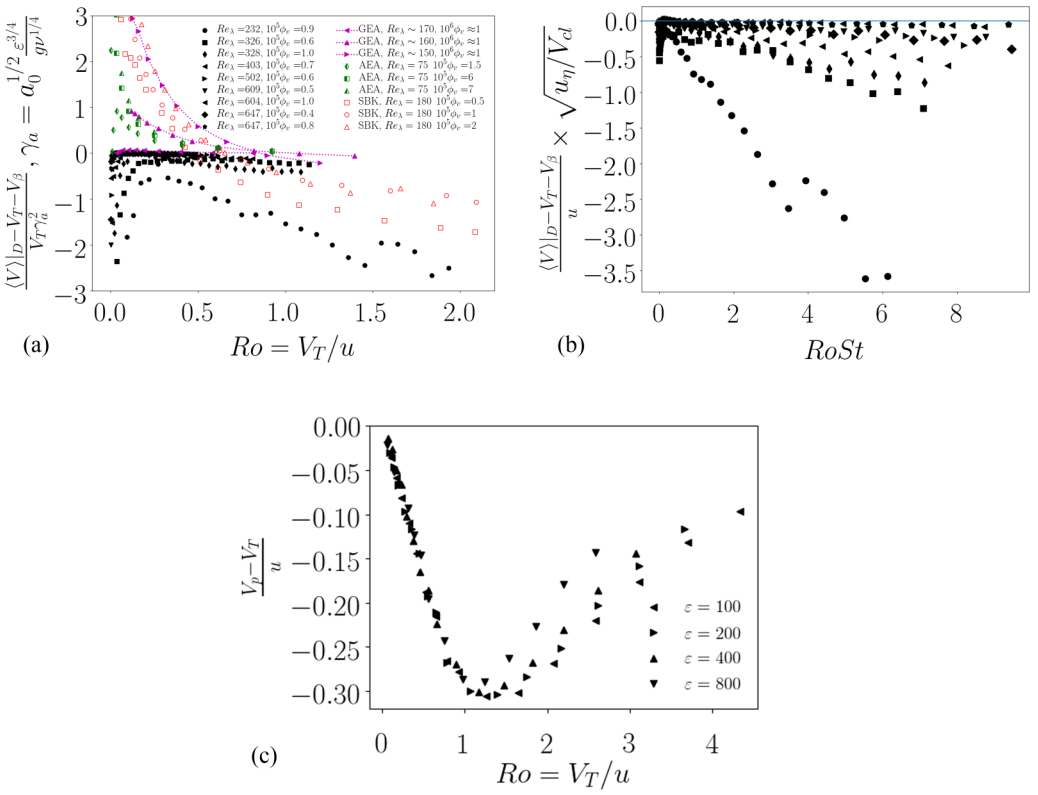

FIG. 13. (a) Sumbekova *et al.* scaling [18]. (b) Combination of the velocity scales for the AG data. (c) Data from Fig. 16 of Rosa *et al.* [28]. In the legends, GEA corresponds to the data of Good *et al.* [29], AEA refers to the data of Aliseda *et al.* [24], and SBK refers to the data of Sumbekova [18].

[1] A. Aliseda and J. Lasheras, Effect of buoyancy on the dynamics of a turbulent boundary layer laden with microbubbles, J. Fluid Mech. **559**, 307 (2006).

[2] P. A. Vaillancourt and M. Yau, Review of particle-turbulence interactions and consequences for cloud physics, Bull. Am. Meteorol. Soc. **81**, 285 (2000).

[3] S. Sumbekova, A. Cartellier, A. Aliseda, and M. Bourgoin, Preferential concentration of inertial sub-Kolmogorov particles: The roles of mass loading of particles, Stokes numbers, and Reynolds numbers, Phys. Rev. Fluids **2**, 024302 (2017).

[4] S. Balachandar and J. K. Eaton, Turbulent dispersed multiphase flow, Annu. Rev. Fluid Mech. **42**, 111 (2010).

[5] A. Aliseda and J. Lasheras, Preferential concentration and rise velocity reduction of bubbles immersed in a homogeneous and isotropic turbulent flow, Phys. Fluids **23**, 093301 (2011).

[6] S. Elghobashi, Direct numerical simulation of turbulent flows laden with droplets or bubbles, Annu. Rev. Fluid Mech. **51**, 217 (2019).

[7] M. Maxey, The gravitational settling of aerosol particles in homogeneous turbulence and random flow fields, J. Fluid Mech. **174**, 441 (1987).

[8] A. D. Bragg, P. J. Ireland, and L. R. Collins, Mechanisms for the clustering of inertial particles in the inertial range of isotropic turbulence, Phys. Rev. E **92**, 023029 (2015).

[9] S. Coleman and J. Vassilicos, A unified sweep-stick mechanism to explain particle clustering in two-and three-dimensional homogeneous, isotropic turbulence, Phys. Fluids **21**, 113301 (2009).

[10] M. Obligado, T. Teitelbaum, A. Cartellier, P. Mininni, and M. Bourgoin, Preferential concentration of heavy particles in turbulence, J. Turbulence **15**, 293 (2014).
[11] S. Goto and J. Vassilicos, Self-similar clustering of inertial particles and zero-acceleration points in fully developed two-dimensional turbulence, Phys. Fluids **18**, 115103 (2006).
[12] S. Ghosh, J. Dávila, J. C. R. Hunt, A. Srdic, H. J. S. Fernando, and P. R. Jonas, How turbulence enhances coalescence of settling particles with applications to rain in clouds, Proc. R. Soc. A **461**, 3059 (2005).
[13] L.-P. Wang and M. R. Maxey, Settling velocity and concentration distribution of heavy particles in homogeneous isotropic turbulence, J. Fluid Mech. **256**, 27 (1993).
[14] P. Nielsen, Turbulence effects on the settling of suspended particles, J. Sediment. Res. **63**, 835 (1993).
[15] P. Nielsen, On the motion of suspended sand particles, J. Geophys. Res. Oceans **89**, 616 (1984).
[16] K. Kawanisi and R. Shiozaki, Turbulent effects on the settling velocity of suspended sediment, J. Hydraul. Eng. **134**, 261 (2008).
[17] J. Tom and A. D. Bragg, Multiscale preferential sweeping of particles settling in turbulence, J. Fluid Mech. **871**, 244 (2019).
[18] S. Sumbekova, A. H. Cartellier, M. Bourgoin, and A. Aliseda, Enhancement versus hindering: impact of the turbulence characteristics on the settling behavior of heavy sub-Kolmogorov particles in a turbulent flow, in *Proceedings of the 10th International Conference on Multiphase Flow (ICMF'19)* (Rio de Janeiro, Brazil, 2019).
[19] S. Sumbekova, A. Aliseda, A. Cartellier, and M. Bourgoin, Clustering and settling of inertial particles in turbulence, in *Proceedings of the 5th International Conference on Jets, Wakes and Separated Flows (ICJWSF'15)* (Springer, Berlin, 2016), pp. 475–482.
[20] R. Monchaux and A. Dejoan, Settling velocity and preferential concentration of heavy particles under two-way coupling effects in homogeneous turbulence, Phys. Rev. Fluids **2**, 104302 (2017).
[21] L. Baker, A. Frankel, A. Mani, and F. Coletti, Coherent clusters of inertial particles in homogeneous turbulence, J. Fluid Mech. **833**, 364 (2017).
[22] P. Huck, C. Bateson, R. Volk, A. Cartellier, M. Bourgoin, and A. Aliseda, The role of collective effects on settling velocity enhancement for inertial particles in turbulence, J. Fluid Mech. **846**, 1059 (2018).
[23] A. J. Petersen, L. Baker, and F. Coletti, Experimental study of inertial particles clustering and settling in homogeneous turbulence, J. Fluid Mech. **864**, 925 (2019).
[24] A. Aliseda, A. Cartellier, F. Hainaux, and J. C. Lasheras, Effect of preferential concentration on the settling velocity of heavy particles in homogeneous isotropic turbulence, J. Fluid Mech. **468**, 77 (2002).
[25] T. Bosse, L. Kleiser, and E. Meiburg, Small particles in homogeneous turbulence: Settling velocity enhancement by two-way coupling, Phys. Fluids **18**, 027102 (2006).
[26] T. Wittemeier and J. S. Shrimpton, Explanation of differences in experimental and computational results for the preferential concentration of inertial particles, Comput. Fluids **173**, 37 (2018).
[27] P. J. Ireland, A. D. Bragg, and L. R. Collins, The effect of Reynolds number on inertial particle dynamics in isotropic turbulence. Part 1. Simulations without gravitational effects, J. Fluid Mech. **796**, 617 (2016).
[28] B. Rosa, H. Parishani, O. Ayala, and L.-P. Wang, Settling velocity of small inertial particles in homogeneous isotropic turbulence from high-resolution DNS, Int. J. Multiphase Flow **83**, 217 (2016).
[29] G. H. Good, P. J. Ireland, G. P. Bewley, E. Bodenschatz, L. R. Collins, and Z. Warhaft, Settling regimes of inertial particles in isotropic turbulence, J. Fluid Mech. **759**, R3 (2014).
[30] B. Rosa, J. Pozorski, and L.-P. Wang, Effects of turbulence modulation and gravity on particle collision statistics, Int. J. Multiphase Flow **129**, 103334 (2020).
[31] D. O. Mora, A. Cartellier, and M. Obligado, Experimental estimation of turbulence modification by inertial particles at moderate Re_λ, Phys. Rev. Fluids **4**, 074309 (2019).
[32] R. Monchaux, M. Bourgoin, and A. Cartellier, Preferential concentration of heavy particles: A Voronoï analysis, Phys. Fluids **22**, 103304 (2010).
[33] M. Obligado, A. Cartellier, and M. Bourgoin, Experimental detection of superclusters of water droplets in homogeneous isotropic turbulence, Europhys. Lett. **112**, 54004 (2015).
[34] D. O. Mora and M. Obligado, Estimating the integral length scale on turbulent flows from the zero crossings of the longitudinal velocity fluctuation, Exp. Fluids **61**, 199 (2020).

[35] L. Mydlarski, A turbulent quarter century of active grids: From Makita (1991) to the present, Fluid Dynam. Res. **49**, 061401 (2017).
[36] D. O. Mora, E. Muñiz Pladellorens, P. Riera Turró, M. Lagauzere, and M. Obligado, Energy cascades in active-grid-generated turbulent flows, Phys. Rev. Fluids **4**, 104601 (2019).
[37] W. Bachalo and M. Houser, Phase/doppler spray analyzer for simultaneous measurements of drop size and velocity distributions, Optic. Eng. **23**, 235583 (1984).
[38] A. J. Puga and J. C. LaRue, Normalized dissipation rate in a moderate Taylor-Reynolds number flow, J. Fluid Mech. **818**, 184 (2017).
[39] S. Sumbekova, Concentration préférentielle de particules inertielles: La structure et la dynamique de clusters, Ph.D. thesis, Universite Grenoble Alpes, 2016.
[40] J. D. Schwarzkopf, M. Sommerfeld, C. T. Crowe, and Y. Tsuji, *Multiphase Flows with Droplets and Particles* (CRC Press, Boca Raton, FL, 2011).
[41] S. Elghobashi, On predicting particle-laden turbulent flows, Appl. Sci. Res. **52**, 309 (1994).
[42] S. B. Pope, *Turbulent Flows* (Cambridge University Press, Cambridge, UK, 2000).
[43] R. Clift, J. Grace, and M. Weber, *Bubbles, Drops, and Particles* (Dover Publications, Mineola, NY, 1978).
[44] J.-S. Ferenc and Z. Néda, On the size distribution of poisson Voronoi cells, Physica A **385**, 518 (2007).
[45] D. O. Mora, A. Aliseda, A. Cartellier, and M. Obligado, Characterizing 1D inertial particle clustering, arXiv:1906.09896.
[46] J. Bec, H. Homann, and S. S. Ray, Gravity-Driven Enhancement of Heavy Particle Clustering in Turbulent Flow, Phys. Rev. Lett. **112**, 184501 (2014).
[47] H. W. Liepmann and M. S. Robinson, Counting Methods and Equipment for Mean-Value Measurements in Turbulence Research (National Advisory Committee for Aeronautics, Washington, DC, 1953).
[48] K. Sreenivasan, A. Prabhu, and R. Narasimha, Zero-crossings in turbulent signals, J. Fluid Mech. **137**, 251 (1983).
[49] N. Mazellier and J. Vassilicos, The turbulence dissipation constant is not universal because of its universal dependence on large-scale flow topology, Phys. Fluids **20**, 015101 (2008).
[50] J. C. Vassilicos, Dissipation in turbulent flows, Annu. Rev. Fluid Mech. **47**, 95 (2015).
[51] Y. Akutina, T. Revil-Baudard, J. Chauchat, and O. Eiff, Experimental evidence of settling retardation in a turbulence column, Phys. Rev. Fluids **5**, 014303 (2020).
[52] C. N. Jacobs, W. Merchant, M. Jendrassak, V. Limpasuvan, R. Gurka, and E. E. Hackett, Flow scales of influence on the settling velocities of particles with varying characteristics, PLoS ONE **11**, e0159645 (2016).
[53] G. Good, S. Gerashchenko, and Z. Warhaft, Intermittency and inertial particle entrainment at a turbulent interface: The effect of the large-scale eddies, J. Fluid Mech. **694**, 371 (2012).
[54] B. Sawford, Reynolds number effects in Lagrangian stochastic models of turbulent dispersion, Phys. Fluids A **3**, 1577 (1991).
[55] M. Obligado, A. Cartellier, A. Aliseda, T. Calmant, and N. de Palma, Study on preferential concentration of inertial particles in homogeneous isotropic turbulence via big-data techniques, Phys. Rev. Fluids **5**, 024303 (2020).
[56] V. Boddapati, M. Manish, and S. Sahu, A novel approach for conditional measurement of droplet size distribution within droplet clusters in sprays, Exp. Fluids **61**, 42 (2020).
[57] Y. Wang and K. M. Lam, Clustering behavior and settling velocity of bidisperse inertial particles in turbulent open channel flow, Int. J. Multiphase Flow **129**, 103303 (2020).